Physical Limits of Power Density Improvements of Electric Machines

Sebastian Mönninghoff
Institute of Electrical Machines (IEM)
RWTH Aachen University
Aachen, Germany
sebastian.moenninghoff@iem.rwth-aachen.de

Kevin Jansen
Institute of Electrical Machines (IEM)
RWTH Aachen University
Aachen, Germany
kevin.jansen@iem.rwth-aachen.de

Kay Hameyer
Institute of Electrical Machines (IEM)
RWTH Aachen University
Aachen, Germany

2023 IEEE International Electric Machines & Drives Conference (IEMDC) | 979-8-3503-9899-1/23/$31.00 ©2023 IEEE | DOI: 10.1109/IEMDC55163.2023.10238899

***Abstract*—Electric traction and propulsion powertrains benefit from machines with high power density. However there are physically reasoned limitations to the improvement of power density in electric machines. In this paper an analytical machine model is used to gain insights into interdependencies between machine sizing variables and their effect on power density. Limits, which can be attributed to available materials and underlying physical effects are identified and compared to the current state of the art. The paper offers the possibility to identify possible improvements due to materials or geometric variations.**

***Index Terms*—machine design principles, power density, pmsm, propulsion, traction**

I. Introduction

The use of electric machines in traction or propulsion applications usually imposes demanding requirements onto the quantity of power density. The achievable power density is however limited. The amount of material, which is required to enable the conversion from electric to mechanic energy in the air gap depends on the machine's topology, the effectiveness of the cooling system, the properties of the components' materials and the operating point, at which the conversion takes place as authors in [1], [2], [3] and [4] point out.

Conducting in depth numerical simulations of all possible machine configurations for a certain machine design task is a prohibitively time consuming and computation intensive task. An analytical formulation of the power density problem as proposed in the course of this work offers the advantage of power density estimations for a wide range of machine configurations. At the same time it promotes machine designs, which are based on an intrinsic understanding of the entire solution range rather than on numerical optimization schemes, where convergence behavior on the global level is often difficult to assess and ensure. While an analytical formulation lacks the precision of finite element simulations, it narrows down the range of possible solutions to a degree, where detailled numerical simulations can be conducted with a reasonable temporal and computational effort.

Authors [5], [6] and [7] show, that design parameters such as the split ratio or the aspect ratio can be used to optimize an electric machine with respect to certain design goals. These approaches however exclude the effect of a machine's inactive mass and do not give estimates for gravimetric power density. This work considers the inactive mass and estimates the resulting gravimetric power density in a similar way as [8]. Authors in [8] elaborate on the combination of highspeed machines with combined gearboxes at the example of four machines and give detailled insights into the combined power density of electric machine and gearbox for each example. This work aims to provide a general overview of how machine design parameters affect the gravimetric power density of electric machines and the physical constraints that limit these parameters.

An analytical machine design approach was chosen based on [5] and [6]. Geometric properties are derived from a set of design parameters. These geometric properties are then used to estimate the mass of the machine. The power density is calculated by using the mass and the power of the machine, which is considered a known design parameter in the course of this work since it directly results from the requirements of the machine design task.

Further studies of the design parameters are performed to obtain general boundary conditions, which can be used to study the physical limitations of the power density of a permanent magnet synchronous machine as shown in fig. 1.

II. Power Density

A. Geometry

The design method from [6] is used to determine the geometry of the machine shown in fig. 1. Equations (1), (2), (3) and (4) are used to derive the air gap diameter D and the active length of the machine l_{act}.

The machine's inner power P, the speed n and the inner torque T are specified by the design task and are therefore treated as boundary conditions. The torque can be further broken down to electromagnetic and geometric properties with the concept of tangential air gap force density σ as shown in (2). To determine the air gap dimensions D and l_{act} the aspect ratio λ is introduced in (3) with the active length l_{act} and the pole pitch τ_p (4).

$$P_i = T_i 2\pi n \tag{1}$$

$$T_i = \sigma(\pi D l_{act})(\frac{D}{2}) \tag{2}$$

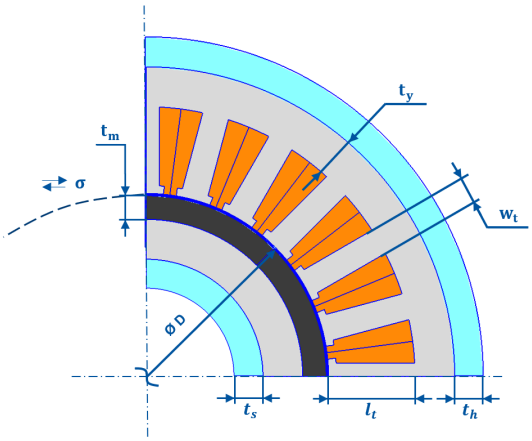

Fig. 1: Machine geometry.

$$\lambda = \frac{l_{act}}{\tau_p} \tag{3}$$

$$\tau_p = \frac{\pi}{p} D \tag{4}$$

The aspect ratio λ of electric machines is used in the design process of electric machines, because it is closely related to thermal design aspects and only varied in a certain range [5], [6]. Other authors also use the ratio $\frac{l}{D}$ [5], [9] for this purpose. Suggestions for suitable choices of $\frac{l}{D}$ are however related to the number of polepairs again [9]. The split ratio $\frac{D_{is}}{D_{os}}$ is also used to optimize electric machines [7], where D_{is} is the inner stator diameter and D_{os} is the outer stator diameter. The approach chosen in this work includes the number of polepairs p into the aspect ratio directly in accordance to [6] to account for its influence as shown in (3). By doing so λ can be used as a design variable to describe the relation between air gap diameter D (5), and active air gap length l_{act} (6):

$$D = \sqrt[3]{\frac{P 2p}{\lambda n \sigma \pi^3}} \tag{5}$$

$$l_{act} = \lambda \frac{\pi D}{2p} \tag{6}$$

The tangential air gap force density σ can be calculated from the linear current density A, the air gap flux density B_δ and the winding factor ξ. A and B_δ are the rms values of the spatial fundamental. The winding factor ξ is assumed to be 1 to achieve the maximum power density. The linear current density A and the air gap flux density B_δ can be constrained by thermal and electromagnetic considerations. Effects on the end-winding of alternative slot and polepair combinations are neglected.

$$\sigma = \xi A B_\delta \tag{7}$$

The geometric dimension for yoke thickness t_y and the tooth width w_t is determined by (8) and (9):

$$t_y = \frac{\pi D}{4p} \cdot \frac{B_\delta}{B_y} \tag{8}$$

$$w_t = \frac{\pi}{Q} D \cdot \frac{B_\delta}{B_y} \tag{9}$$

where B_δ denotes the air gap flux and B_t and B_y denote flux densities in stator teeth and yokes.

Choosing the tooth width according to (9) ensures that teeth are not saturated. Since the stator winding and the teeth compete for the available space in the stator, the length of the teeth has to be chosen so that the required linear current density A can be provided. This condition is expressed by (10) with τ_Q as the slot pitch (11), A_{slot} as the cross sectional area of a slot, k_{cf} as the copper fill factor, J_c as the conductor current density and Q as the number of stator teeth. The length of the teeth l_t can be calculated with (12), which takes into account, that the slot width increases due to the choice of parallel flanked stator teeth.

$$A \tau_Q = A_{slot} J_c k_{cf} \tag{10}$$

$$\tau_Q = \frac{\pi D}{Q} \tag{11}$$

$$l_t = \sqrt{\left(\frac{D}{2} - \frac{B_\delta D}{2B_t}\right)^2 + \frac{AD}{Jk_{cf}}} - \left(\frac{D}{2} + \frac{B_\delta D}{2B_t}\right) \tag{12}$$

The machine is assumed to be a hollow cylinder with a homogenous density, outer stator diameter D_o (13) and inner rotor diameter D_i (14):

$$D_o = D + 2l_t + 2t_y \tag{13}$$

$$D_i = D - 2h_{pm} - 2t_y \tag{14}$$

with magnet height h_{pm}. The height of the magnet is chosen to prevent irreversible demagnetization at the trailing magnet edge according to [10](15), where H_{max} is an acceptable negative magnetic field strength, which does not cause irreversible demagnetization and δ is the air gap width:

$$h_{pm} = \frac{A \cdot \tau_p}{2H_{max}} - \delta \tag{15}$$

B. Mass Estimation

A simplified mass calculation (16) can be derived by assuming, that the machine's active cross sectional area can be linearized and calculated as a rectangle with the air gap circumference πD as length and the height $\frac{D_o - D_i}{2}$. In a first step the achievable power density $\frac{P}{m_{act}}$ is defined by the machine's output power and its electromagnetically active mass as shown in (17).

$$m_{act} = \rho l_{act} \pi D (2t_y + h_{pm} + l_t) \tag{16}$$

$$\frac{P}{m_{act}} = \frac{P}{\rho l_{act} \pi D (2t_y + h_{pm} + l_t)} \tag{17}$$

Equation (17) estimates unrealistically high power densities if λ is chosen infinitesimally small, because the electromagnetically inactive mass is not considered in (17). This enables a very short machine with a large air gap diameter without end-winding or other inactive components. Theoretically it would

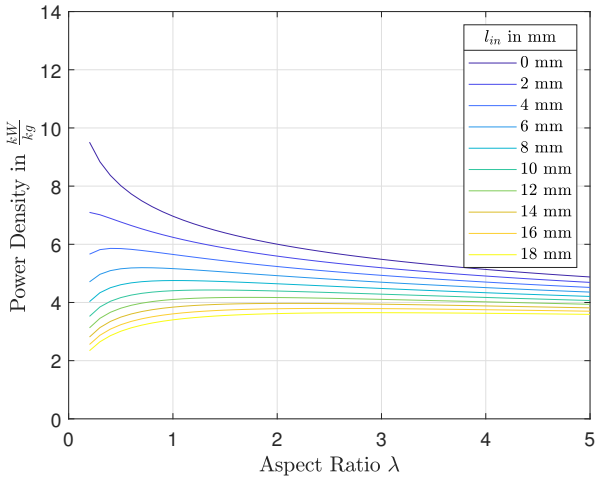

Fig. 2: Effect of inactive length on power density.

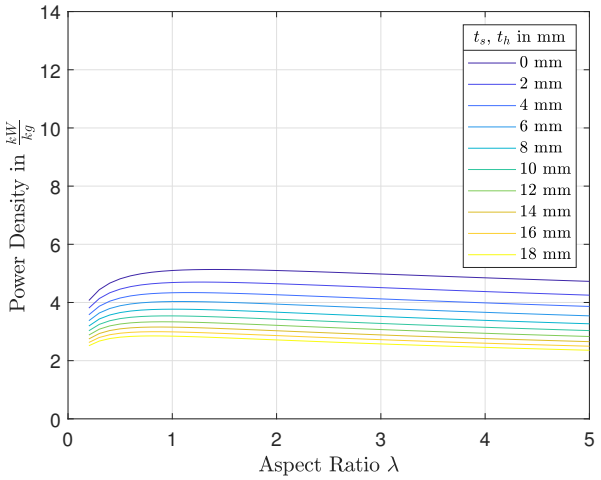

Fig. 3: Effect of shaft and housing thickness on power density.

be beneficial to build machines with very low λ, if the weight of the electromagnetically inactive mass is infinitesimally small. In reality such machines are not practical, because end-windings, bearings, cooling systems and the precise positioning between rotor and stator by a housing are necessary. The effect of flux leakage would also disencourage such machine designs. Furthermore, the linearized cross section calculation leads to significant errors for small D and different thicknesses between rotor and stator.

Therefore, to achieve realistic estimates for the power density, the inactive mass has to be considered. An improved mass calculation (18) is used, which considers the effect of inactive machine mass by penalties to active length l_{act} and diameters D_i, D_o. The improved mass calculation (18) does not use linearization to calculate the machine volume.

$$m_{tot} = \rho(l_{act} + l_{in})\frac{\pi}{4}((D_o + 2t_h)^2 - (D_i - 2t_s)^2) \quad (18)$$

$$\frac{P}{m_{tot}}(P, n, p, A, B_{ag}, \lambda, J, k_{cf}, B_y, B_t, f_{dl}, f_{dth}, f_{dts}) = \frac{P}{\rho(l_{act} + 2l_{in})\frac{\pi}{4}((D_o + 2t_h)^2 - (D_i - 2t_s)^2)} \quad (19)$$

$$l_{in} = D_o \cdot f_{dl} \quad (20)$$

$$t_h = l \cdot f_{dth} \quad (21)$$

$$t_s = l \cdot f_{dts} \quad (22)$$

The shaft thickness t_s, housing thickness t_h and inactive length l_{in} are introduced to estimate the electromagnetically inactive mass of the machine. The power density estimation (19) can now be formulated, which includes the total mass of the machine. The inactive length introduces a penalty for machines with small l_{act} and results in unfavorable ratios $\frac{m_{act}}{m_{tot}}$ for small λ. As a consequence the achievable power density $\frac{P}{m_{tot}}(\lambda)$ develops a maximum as shown in fig. 2. The curve exhibits a sharp decrease in power density for lower λ and a rather slow decrease for large λ. This offers the possibility to design longer machines with smaller air gap diameters while power density decreases by an acceptable amount. This characteristic is important, if the circumferential speed of the rotor has to be reduced to ensure mechanical integrity. For realistic parametrization of (19) the power density maximum occurs between 0.5 and 3, depending on the other parameters of (19), which is in the range of suggested values given in [6] and [9]. The effect of shaft thickness t_s and housing thickness t_h is demonstrated in fig. 3. Both disencourage the choice of large λ, which gives long machines with small air gap diameters. This trend can also be observed without any inactive mass and is further amplified by the introduction of t_s and t_h. If not stated otherwise, the optimal λ is always chosen when varying other design variables throughout this work. Although assuming realistic but constant values for t_s, t_h and l_{in} does already provide useful power density estimations over a wide parameter range, the approach can be refined by introducing dependencies of these quantities on the main geometric machine dimensions. This takes growth characteristic estimations for these inactive components into account as shown in (20), (21) and (22).

III. Limits of Power Density

A. Magnetic Limitation

The tangential air gap force density is proportional to $A \cdot B_\delta$. Available space in radial flux machine stators is used by the winding system, which provides the linear current density A as well as the iron core, which carries the magnetic flux provided by B_δ. Iron cores with higher values of polarization saturation allow for thinner iron cross sections by reducing t_y (8) and w_t (9), which enables larger slot areas, while carrying the same flux. If the conductor current density J_c is assumed to be fixed by thermal limitations, the increased slot area results in increased capabilities to provide linear current density A. The saturation flux densities for iron cores are however limited

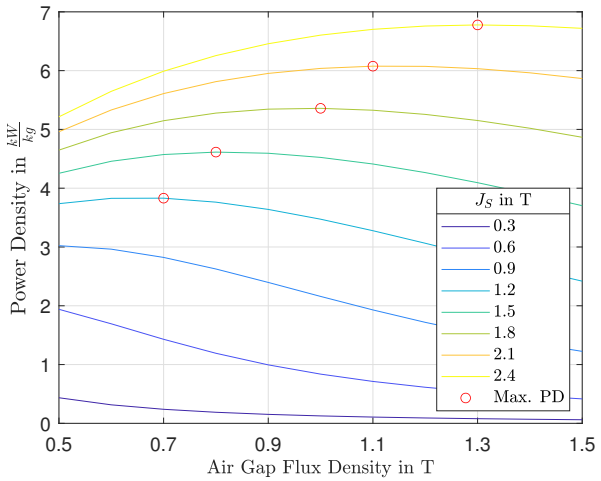

Fig. 4: Effect of air gap flux density and iron saturation on power density.

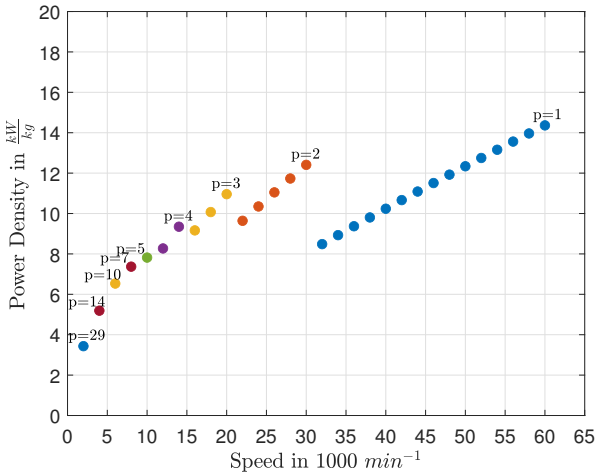

Fig. 5: Effect of fundamental frequency limit on power density.

by available soft magnetic materials [11]. According to [11] iron-cobalt steels offer a state-of-the-art saturation polarization at 2.35 T. The achievable air gap flux density B_δ largely depends on material properties of permanent magnets and the rotor topology. The remanence B_r of the permanent magnetic material is limited by available state of the art material grades to 1.5 T [14]. The effect of stray flux paths are neglected in the course of this work to establish a physical boundary case. The coercivity determines the magnet height, which is required to prevent irreversible demagnetization. Fig. 4 shows, that an optimal air gap flux density exists for a given iron core flux density. The maxima mark the optimal ratio between space occupied by stator teeth and space required by the stator winding.

The yoke size can also be reduced by increasing the number of polepairs. Since power electronics have a limited switching frequency, the electric frequency of the machine is limited. Therefore, the number of polepairs cannot be increased arbitrarily. Another disadvantage of higher polepair number and higher electric frequencies are the increased iron losses as stated in [12] and the increasing influence of cutting-edge material deterioration [13]. If a maximum electric frequency is assumed, while the corner rotational speed of the machine design is increased, an intermittend rise in power density can be observed as shown in fig. 5. The number of polepairs is in this case chosen to be $\lfloor \frac{f_{max}}{n} \rfloor$ with $f_{max} = 1000$ Hz.

B. Thermal Limitations

The winding insulation system may be degraded, if exposed to temperatures above the material rating. Copper and iron losses are in this study considered to be the only contributors to machine losses. As shown in (7) the tangential air gap force density is directly proportional to the linear current density A. A can either be increased by designing larger slots or by increasing the slot current density. Both approaches lead to increased copper losses, which have to be extracted by the cooling system.

Assuming a direct conductor cooling system, the cooling surface area increases proportionally to the slot area, as shown in fig. 6. Thus, increasing the linear electric load A with a constant conductor current density J_c proportionally increases the cooling area. The available cooling area per total ohmic losses is thusly assumed to be independent of A and only depends on the conductor current density J_c, which is an advantage when compared to conventional jacket cooling systems, where the coolable surface does not increase proportionally to the linear current density A. An energy balance for a stator section of one slot pitch τ_Q as shown in fig. 6 leads to (23):

$$\begin{aligned} & m_c c_p dT = \dot{Q}_{L,c} + \dot{Q}_{L,Iron} - \dot{Q}_C \\ \Leftrightarrow & J_{max}(dT, dt) = \sqrt{\frac{\rho_c}{\rho_{el}} \left(\frac{c_p dT}{dt} + \dot{q}_C - \dot{q}_{L,Iron} \right)} \end{aligned} \tag{23}$$

where dT is the temperature difference in the conductor, which occurs during the time period dt. The conductor has the density ρ_c, the gravimetric heat capacity c_p and the electric resistivity ρ_{el}. The conductor deducts heat to the cooling

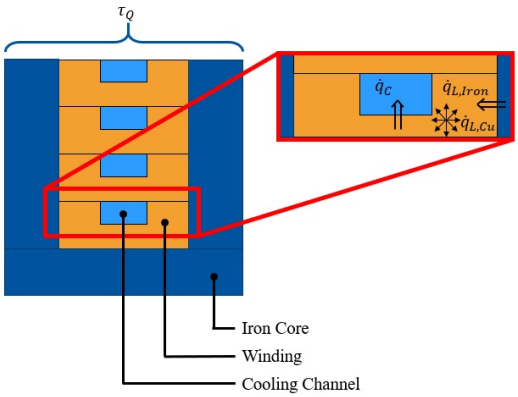

Fig. 6: Thermal balance.

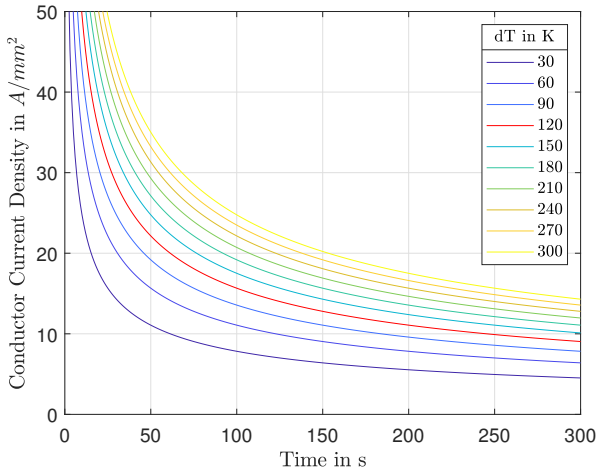

Fig. 7: Sustainable conductor current density during transient operation.

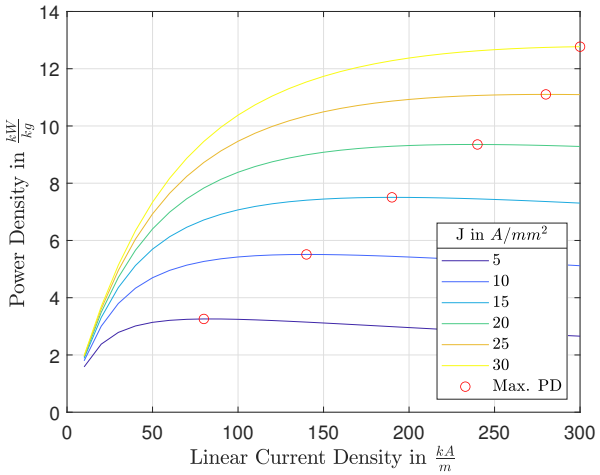

Fig. 8: Effect of conductor current density and linear current density on power density.

channel $\dot{q}_C$ and is heated up by the surrounding iron core with $\dot{q}_{L,Iron}$.

[16] defines S1 and S2 operating cycles of electric machines, for long- and short term operation. To determine the S2 short time current densities, dT can be determined by considering the maximum adiabatic rise of conductor temperature during time period dt. $\lim_{dt\to\infty} J_{max}(dT, dt)$ reveals an estimation for the feasible S1 current density for continuous operation. Since J_{max} is proportional to $\sqrt{\frac{\rho_c}{\rho_{el}}}$ using silver as a conductor material offers 11.4 % gain in S1 current density in comparison to copper. Heat capacity of silver however is 39,5 % lower than that of copper, which favors copper for S2 short time operation.

Fig. 8 demonstrates the influences of the linear current density A and the conductor current density J_c on the power density. If for a certain linear current density the conductor current density is increased, the power density gain decreases with increasing J_c. Increasing J_c does have no effect on the air gap diameter D but only reduces the required slot area and the required tooth length l_t. This effect is however not affect all machine masses, which means that J_c approaching infinity does not lead to infinitely power dense machines. To increase the power density further an increase of the linear current density is required, since this reduces the air gap diameter by increasing the tangential air gap force density. Increasing A while maintaining a constant J_c does only increase the power density up to a certain maximum. After this maximum is reached a slow but steady decrease in power density can be observed. This effect can be attributed to the the additional mass of the yoke and the additional inactive masses due to increasing slot surfaces, which offset the gain offered by an increase of tangential air gap force density.

C. Mechanical Limitations

The power density of the machine can be increased by increasing the speed as shown in fig. 5. Since the mechanical, tangential rotor stress depends on the rotor surface velocity [15], the rotational speed can not be increased arbitrarily. Considering the formulation of the air gap diameter shown in (5) the achievable rotational speed for a thin rotating ring can be expressed with (24), where R is the equivalent strength of the rotor assembly and ρ the equivalent mass density.

$$n_{max} = \left(\frac{R}{\rho\pi^2}\right)^{\frac{2}{3}} \cdot \sqrt{\frac{\lambda\sigma\pi^2}{2Pp}} \tag{24}$$

The maximum rotational speed is proportional to $\sqrt{\lambda}$, which means λ as a free design variable is restricted by the mechanical strength of the rotor, if the shaft speed is treated as a fixed design boundary condition. In cases with high output power, high number of polepairs and a fixed rotational speed it is not always possible to choose the λ, which leads to the optimaum power density, because low λ lead to a larger air gap diameter and therefore higher circumferential speeds. Machines with higher λ have to be chosen in these cases to decrease the air gap diameter. On the other hand it can be stated, that increasing the rotor assemblies' mechanical strength with e.g. a sleeve or lowering the rotors equivalent density with e.g. fiber-reinforced composites increases the achievable rotational speed. Increasing the tangential air gap force density of the machine does lead to smaller air gap diameters and is also suited to increase the speed limit of a machine design, if the speed is a free design variable.

IV. Market Study

To assess, wether the methodology developed in this paper is able to estimate the achievable power densities of a radial flux PMSM in direct drive configuration, different technological scenarios are defined in tab. I. The power densities, which are determined on the basis of these technology scenarios are then compared to a market study, which is shown in fig. 9. The study includes state of the art electrical machines used in traction and propulsion applications [17] - [35]. Direct drives

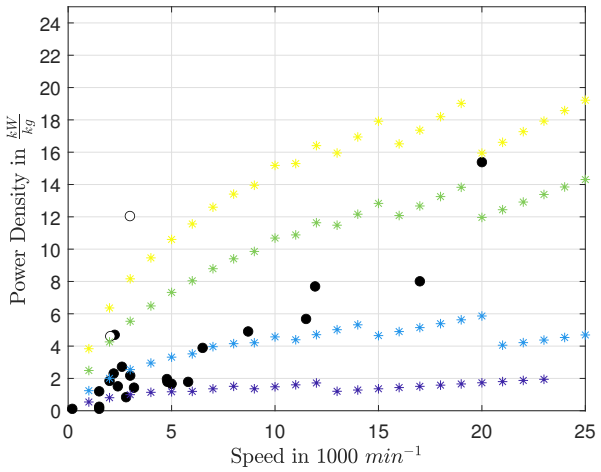

Fig. 9: Market study compared to technology scenarios A.-D. [17] - [35].

a marked with a filled datapoint, whereas indirect drives are marked with just a circle.

TABLE I: Technology Scenarios

Parameter	Unit	Scenario			
		A	***B***	***C***	***D***
P	kW	50	50	50	250
$f_{el,max}$	Hz	$400Hz$	$700Hz$	$1000Hz$	$1000Hz$
A	kA/m	50	100	150	150
k_{cf}	-	0.35	0.45	0.6	0.6
J_c	A/mm²	5	10	15	15
B_δ	T	0.8	0.9	1.1	1.1
B_t	T	1.5	1.7	2.2	2.2
B_y	T	1.5	1.7	2.2	2.2

Operating conditions such as the cooling fluid inlet temperature or the duration of an operating point influence the achievable output power and thereby the achievable power density of an electric machine. Specified durations for short term operation deviate between different manufacturers. This makes a comparison of S2 power densities between different manufacturers difficult. In the course of this market study only S1 power densities were used to increase the comparability of the dataset. Furthermore the corner speed was used for plotting instead of the maximum rotational speed. This takes into consideration, that most electric machines used in traction applications have a large field weakening range. It can be seen, that an increased corner speed enables machines with higher power densities, which is to be expected and predicted by (17). The direct comparison between direct and indirect drive solutions for the same design task on the basis of this dataset is however difficult, since only one machine can be found, where corner speed, power density of the machine with gearbox and power density of the same machine without gearbox is known [34]. The properties for this machine have to be treated with care however, because they are extracted from preliminary tests and not yet validated by a testbench measurement. Another indirect drive solution was found, which also hints at the potential powerdensity improvement by such a concept, but no data was available for the same machine without the gearbox [28], [29]. This machine is designed for the same corner speed as the Siemens SP260D [19], [20] but for a lower power range. The Siemens machine stands out from the dataset as a very power dense direct drive machine. Although there are axialflux machines, which are comparable [36] - [39], these have not been considered within the scope of this work, because the methodology is formulated explicitly for a radial flux PMSM.

Scenarios A.-C. explore the influence of advanced cooling technologies, state of the art materials and winding technology on the power density of the machine, while the output power remains constant. Scenario A. describes a very conservative machine design scenario with pessimistic values for the linear current density A and the copper fill factor k_{cf}. The parameters for soft magnetic materials are conservative estimates for FeSi steel, which result in wider teeth than necessary, longer teeth and larger outer stator diameters. The air gap flux density is varied from 0.8 in scenario A. to 1.1 in scenario C. NdFeB magnets are considered in all scenarios. The increase in air gap flux density from scenario A. to scenario C. takes into account better quality of available NdFeB material grades and improved rotor topologies. The other values for scenario C. are chosen optimistically to reflect advancements in winding technologies, improved cooling technologies and the application of FeCo steels [11]. Scenario D. does explore the effect of incresed output power on the power density.

It can be seen that, the pessimistic and the optimistic case cover the boundaries of the market study. The pessimistic case indicates, that indirect drive configurations are not viable for conservative machine designs, since only small increases in power density are achieved by increasing the corner speed. The additional weight of the gear box will offset these gains. The scenarios B.-D. show a similar characteristic as demonstrated in fig. 5: Due to the limited fundamental frequency, the power density increases intermittedly with decreasing gradient. Significant increases of the corner speed are required as soon as $p = 1$ to achieve further power density gains. The weight of the gear box depends, among other variables, on the transmission ratio. From looking at the dataset given in [34], which corresponds to the direct and indirect drive with the highest power densities in he market study, it can be expected, that the small power density gains achieved by increasing the rotational speed at $p = 1$ are eventually offset by the weight of the gearbox, even for the most optimistic scenario D.

V. Conclusions

An analytical description of the power density for a radial flux PMSM is derived in this work, which offers insights into basic laws governing the power density in PMSM. The model allows an analytical physical interpretation of influences on power density. Using the machine design procedure described in [6] the active mass was determined. Based on estimates regarding the geometric properties of inactive components a total machine mass was estimated and used to estimate the

power density of the machine. Fig. 2 and fig. 3 show, that the inclusion of inactive mass, specifically inactive length, causes the developement of an optimal λ. Interesting findings show, that there exist optimal solutions for combinations of $\frac{P}{m}(J_S,\ B_\delta)$ and $\frac{P}{m}(J_c,\ A)$ as shown in fig. 4 and fig. 8. Limiting the fundamental frequency of the machine results in a decrease of power density gain with increasing rotational speed. In a pessimistic technology scenario this effect offsets any power density advantages, which are gained by increasing the rotational speed of the machine as can be seen in fig. 9. Even in an optimistic scenario it remains questionable, wether the maximization of rotational speed is advantageous if a gearbox is required to adapt to a much lower shaft speed. Choosing the number of polepairs in the range of 2-4 for an indirect drive configuration seems to be more favorable in this case. More detailled design studies are required to determine the best choice.

The heat balance analysis (23) suggests, that copper is better suited for short term applications than silver due to its higher heat capacity, while S1 operation favors silver as a conductor material due to its more favorable $\sqrt{\frac{\rho_c}{\rho_{el}}}$.

It has to be stated however, that simple analytical models as proposed in this paper suffer from uncertainties. Furthermore important influences like skin effect, rotor cooling and winding factor are neglected and to be considered in more detailled studies. The methodology proposed in this paper can be reformulated for different machine topologies which might enable a very fundamental approach to explore and compare different topological solutions for a certain machine design task.

ACKNOWLEDGMENT

The contribution of S. Mönninghoff to this work originated as part of the research project "eSAT" (OP EFRE EFRE-0801691; AZ Leitmarkt Agentur ML-2-2-018J ESAT).

REFERENCES

[1] J. Swanke, D. Bobba, T.M. Jahns, and B. Sarlioglu, "Comparison of modular PM propulsion machines for high power density". in 2019 IEEE Transportation Electrification Conference and Expo, June 2019, pp. 1-7.

[2] M. Henke, G. Narjes, J. Hoffmann, C. Wohlers, S. Urbanek, C. Heister, and B. Ponick, "Challenges and opportunities of very light high-performance electric drives for aviation" in Energies, 11(2), 2018, p. 344.

[3] A. El-Refaie, "Role of advanced materials in electrical machines", in CES Transactions on Electrical Machines and Systems, 3(2), 2019, 124-132.

[4] A. D. Anderson, N. J. Renner, Y. Wang, S. Agrawal, S. Sirimanna, D. Lee, and J.L. Felder, "System weight comparison of electric machine topologies for electric aircraft propulsion" in AIAA/IEEE Electric Aircraft Technologies Symposium (EATS), 2018 , pp. 1-16.

[5] T. A. Lipo, "Introduction to AC machine design", John Wiley and Sons, 2017.

[6] G. Müller, K. Vogt, B. Ponick, "Berechnung elektrischer Maschinen", John Wiley and Sons, 2012.

[7] V. B. Honsinger, "Sizing equations for electrical machinery", IEEE Transactions on Energy Conversion, 1987, Nr. 1, pp. 116-121.

[8] D. Schweigert, M. E. Gerlach, A. Hoffmann, B. Morhard, A. Tripps, T. Lohner, K. Stahl, "On the Impact of Maximum Speed on the Power Density of Electromechanical Powertrains", Vehicles, 2(2), 365-397, 2020.

[9] J. Pyrhonen, T. Jokinen, V. Hrabovcova, "Design of rotating electrical machines", John Wiley and Sons, 2013.

[10] A. Binder, "Elektrische maschinen und antriebe", 2012.

[11] F. Fiorillo, G. Bertotti, C. Appino, and M. Pasquale, "Soft magnetic materials" in Wiley Encyclopedia of Electrical and Electronics Engineering, John Wiley and Sons, Inc., 2016, pp. 1-42.

[12] S. Steentjes, M. Leßmann, and K. Hameyer, "Semi-physical parameter identification for an iron-loss formula allowing loss-separation" in Journal of Applied Physics, Vol. 113 No. 17, 2013, p. 17A319.

[13] H. A. Weiss, N. Leuning, S. Steentjes, K. Hameyer, T. Andorfer, S. Jenner, and W. Volk, "Influence of shear cutting parameters on the electromagnetic properties of non-oriented electrical steel sheets" in Journal of Magnetism and Magnetic materials, 421, 2017, pp. 250-259.

[14] S. Hirosawa, M. Nishino, and S. Miyashita, "Perspectives for high-performance permanent magnets: applications, coercivity, and new materials" in Advances in Natural Sciences: Nanoscience and Nanotechnology, 8(1), 2017, 013002.

[15] B. Riemer, M. Leßmann, and K. Hameyer, "Rotor design of a high-speed permanent magnet synchronous machine rating 100,000 rpm at 10kW" in IEEE Energy Conversion Congress and Exposition, September 2010, pp. 3978-3985.

[16] International Electrotechnical Commission, "IEC 60034-1: rotating electrical machines, Part 1: Rating and performance", International Electrotechnical Commission: London, UK, 2010.

[17] Plettenberg , "Nova 15/50/B3 S P30 HF", https://plettenbergmotors.com/product/nova-15-en/ (accessed Mar. 24, 2023).

[18] Plettenberg , "Nova 30", https://plettenbergmotors.com/deutsch/product/nova-30/ (accessed Mar. 24, 2023).

[19] k: Petermaier, "Electric propulsion components with high power densities for aviation", In Transformative Vertical Flight Workshop (Vol. 2, pp. 1-16), Mar. 2015.

[20] F. Anton, "eAircraft: Hybrid-elektrische Antriebe für Luftfahrzeuge", 14. Tag der Deutschen Luft- und Raumfahrtregionen, 2019.

[21] Rotex, "Rotex REB 90", https://www.rotexelectric.eu/products/bldc-motors/reb-series/ (accessed Mar. 24, 2023).

[22] Geiger Engineering, "Manual - Complete electric drive system V1.92", https://www.geigerengineering.de (accessed Mar. 24, 2023).

[23] Oswald Elektromotoren GmbH, "MF Synchronmotoren /-Generatoren", https://www.oswald.de (accessed Mar. 24, 2023).

[24] Alxion, "Alxion 300STK8M", http://alxion.com (accessed Mar. 24, 2023).

[25] VEM, "VEM IE4-PE1R 160 M4", https://www.vem-group.com/ (accessed Mar. 24, 2023).

[26] Sineton, "Sineton A37K154", https://electricmotorglider.com/2016/02/16/72-40-sineton-a37k154-electric-motor/ (accessed Mar. 24, 2023).

[27] Bosch, "Bosch SMG 180", https://www.bosch-mobility-solutions.com/en/solutions/electric-motors/separate-motor-generator-ohw/ (accessed Mar. 24, 2023).

[28] D. Siegler, "Another Combined Motor-Controller System", Sustainable Skies, https://sustainableskies.org/another-combined-motor-controller-system/ (accessed Mar. 24, 2023).

[29] Schaeffler, "Hybridisierungsbaukasten", https://www.schaeffler-engineering.com (accessed Mar. 24, 2023).

[30] J. Merwerth, "The Hybrid-Synchronous Machine of the new BMW i3 and i8", Challenges with Electric Traction Drives for Vehicles Workshop, University Lund.

[31] J. Doerr, T. Attensperger, L. Wittmann, "The New Electric Axle Drives from Audi", MTZ Worldw 79, 2018, pp. 18–25.

[32] P. Lück, K. Bennewitz, J. Tousen, "Volkswagen's electric drivetrains of the new modular e-drive kit (MEB)" Volkswagen AG, 19th International VDI CongressDritev – Drivetrain for Vehicles, VDI Berichte Nr. 2354., pp.517-530.

[33] AVID technology, "AVID AF130", Datasheet.

[34] H3X1, "HPDM-250 Datasheet version 1.7", https://www.h3x.tech/ (accessed Mar. 24, 2023).

[35] SciMo, "SciMo SY43", https://sci-mo.de/ (accessed Mar. 24, 2023).

[36] Emrax, "Emrax 188", https://emrax.com/e-motors/emrax-188/ (accessed Mar. 24, 2023).

[37] Emrax, "Emrax 268", https://emrax.com/e-motors/emrax-268/ (accessed Mar. 24, 2023).

[38] Yasa, "Yasa 750 R", https://www.yasa.com/wp-content/uploads/2021/05/YASA-750RDatasheet-Rev-11.pdf (accessed Mar. 24, 2023).

[39] Yasa, "Yasa P400 RS", https://www.yasa.com/wp-content/uploads/2021/05/YASA-P400RDatasheet-Rev-14.pdf (accessed Mar. 24, 2023).